

# Determination of Accurate $^{19}\text{F}$ Chemical Shift Tensors with R-Symmetry Recoupling at High MAS Frequencies (60-100 kHz)

Gal Porat-Dahlerbruch<sup>1</sup>, Jochem Struppe<sup>2</sup>, Caitlin M. Quinn<sup>1</sup>, Angela M. Gronenborn<sup>1,3,4</sup>, Tatyana Polenova<sup>1,3,4</sup>

<sup>1</sup>Department of Chemistry and Biochemistry, University of Delaware, Newark, Delaware 19716, United States; <sup>2</sup>Bruker Biospin Corporation, 15 Fortune Drive, Billerica, MA 01821, United States; <sup>3</sup>Department of Structural Biology, University of Pittsburgh School of Medicine, 3501 Fifth Ave., Pittsburgh, PA 15261, United States; <sup>4</sup>Pittsburgh Center for HIV Protein Interactions, University of Pittsburgh School of Medicine, 1051 Biomedical Science Tower 3, 3501 Fifth Avenue, Pittsburgh, PA 15261, United States

**\*Corresponding author:** Tatyana Polenova, Department of Chemistry and Biochemistry, University of Delaware, Newark, DE, USA, Tel.: (302) 831-1968; Email: [tpolenov@udel.edu](mailto:tpolenov@udel.edu)

**Keywords:** high-frequency  $^{19}\text{F}$  MAS NMR, R-symmetry recoupling, chemical shift anisotropy

## Abstract

Fluorination is a versatile and valuable modification for numerous systems, and  $^{19}\text{F}$  NMR spectroscopy is the premier method for their structural characterization.  $^{19}\text{F}$  chemical shift anisotropy is a sensitive probe of structure and dynamics, even though  $^{19}\text{F}$  chemical shift tensors have been reported for only a handful of systems to date. Here, we explore  $\gamma$ -encoded R-symmetry based recoupling sequences for the determination of  $^{19}\text{F}$  chemical shift tensors in fully protonated organic solids at high, 60-100 kHz MAS frequencies. We show that the performance of  $^{19}\text{F}$ -RNCSA experiments improves with increasing MAS frequencies, and that  $^1\text{H}$  decoupling is required to determine accurate chemical shift tensor parameters. In addition, these sequences are tolerant to  $B_1$ -field inhomogeneity making them suitable for a wide range of systems and experimental conditions.

## 1. Introduction

High sensitivity, high natural abundance, and the lack of background signals make  $^{19}\text{F}$  an attractive probe for studies of organic and biological systems by NMR spectroscopy [1-3]. Fluorinated moieties are common in pharmaceuticals [4-6] and can be readily incorporated into proteins and nucleic acids for NMR studies [1]. The  $^{19}\text{F}$  chemical shift tensor (CST) is exquisitely sensitive to the local electronic environment, structure, and dynamics. In general, CSTs for spin-1/2 nuclei can be measured using different magic-angle spinning (MAS) NMR techniques, including chemical shift anisotropy (CSA) recoupling experiments at slow (below 10 kHz), moderate (10-40 kHz) and fast (above 40 kHz) MAS frequencies [7], while  $^{19}\text{F}$  CSTs have so far been determined mostly from static powder patterns [8-12], spinning sideband patterns at MAS frequencies below 35 kHz [13-21], or recoupling experiments at MAS frequencies below 5 kHz [22, 23]. For example, the MREV-8 recoupling sequence can be used to decouple the  $^{19}\text{F}$ - $^{19}\text{F}$  homonuclear dipolar couplings and Scheler and Harris used this strategy to measure  $^{19}\text{F}$  CSTs of fluorinated adamantane and polyvinylidene fluoride (PVDF) at the MAS frequency of 3 kHz with  $^1\text{H}$  decoupling [22]. Qiang and Schmidt-Rohr implemented MREV-8 in a 2D experiment to measure  $^{19}\text{F}$  CSTs in scarcely protonated polymer samples, polytetrafluoroethylene (PTFE) and Nafion, at the MAS frequency of 2.5 kHz and without  $^1\text{H}$  decoupling [23]. However, these experiments are not applicable when i) strong  $^{19}\text{F}$  homonuclear dipolar couplings are present and distort the line shapes, ii) the molecule contains several  $^{19}\text{F}$  atoms whose resonances overlap, and iii) the concentration of the sample is limited, resulting in low sensitivity. In those circumstances, fast MAS frequencies ( $\geq 60$  kHz) are required.

The R-symmetry based ( $\text{RN}_n^\nu$ ) recoupling experiments introduced by Levitt and coworkers [24-26] do not have an upper limit for MAS frequency. The recoupling blocks are composed of a series of  $N$   $\pi$ -pulses extending over  $n$  rotor periods, with each pulse having an alternating phase of  $\pm(\nu/N)*180^\circ$ . The combination of the three symmetry numbers,  $N$ ,  $n$ , and  $\nu$ , determines which terms in the interaction Hamiltonian are recoupled [24]. Suitable combinations of symmetry numbers can be devised to recouple the CSA at arbitrary conditions [24-28], including high MAS frequencies of 60-111 kHz, which are readily attainable in the current commercial MAS NMR probes. The RNCSA experiments utilize the  $\gamma$ -encoded subset of  $\text{RN}_n^\nu$ -symmetry pulse sequences to recouple either the first-rank ( $\sigma_1$ ) or the second-rank ( $\sigma_2$ ) spatial components of the CSA interaction [27]. While powerful,  $\text{RN}_n^\nu$ -symmetry experiments only inform on the magnitude of the CSA interaction, and the sign of the anisotropy has to be obtained by other methods. Titman and coworkers used the  $\text{R}12_5^4$ -symmetry pulse sequence in a 2D  $^{19}\text{F}$  anisotropic-isotropic correlation spectrum at the MAS frequency of 65 kHz of PVDF with  $^1\text{H}$ - $^{19}\text{F}$  dipolar couplings of 8.6 kHz for nearest proton-fluorine pairs, and showed by simulations that these couplings have no appreciable effect on the recoupled  $^{19}\text{F}$  CSA line shape [29]. However, since the R-symmetry CSA recoupling sequences reintroduce heteronuclear dipolar couplings, for systems containing a large number of hydrogens, such as fluorinated pharmaceuticals and biological assemblies,  $^1\text{H}$  decoupling is required, as shown here.

In this report, we present  $^{19}\text{F}$  RNCSA based experiments for measurements of  $^{19}\text{F}$  CSTs in fully protonated systems at high (60-100 kHz) MAS frequencies. We judiciously selected three samples, a generic formulation of the blockbuster cholesterol-lowering drug Atorvastatin calcium, the antimalarial drug Mefloquine in crystalline form, and crystals of a frequently used fluorinated

amino acid, 5-fluoro-L-tryptophan (5F-L-Trp). These molecules were selected because they contain either a trifluoromethyl group (Mefloquine) or fluorinated aromatic groups (Atorvastatin calcium and 5F-L-Trp), and 5F-L-Trp is commonly introduced into proteins [17, 18, 21, 30-32]. The chemical structures of the molecules under study are shown in Figs. 2a, 3a, and 4a.

For all three samples, we carefully assessed the performance of different  $RN_n^v$  sequences with respect to the spinning frequency,  $^1H$  decoupling schemes, and robustness towards  $B_1$  field homogeneity and off-resonance effects. Our findings are the basis for establishing general experimental conditions for determining accurate  $^{19}F$  CSA parameters in RNCSA experiments and highlight the power of fast MAS frequencies for such experiments.

## 2. Experimental

### 2.1. Sample preparation

Mefloquine hydrochloride was purchased from Acros Organics and used without further recrystallization. Atorvastatin calcium generic formulation (10 mg tablets, 6% w/w active pharmaceutical ingredient) was manufactured by Teva and used as is. The excipients are not fluorinated. Both Mefloquine and Atorvastatin calcium were packed into 0.7 and 1.3 mm MAS rotors. 5F-L-Trp was purchased from Advanced ChemBlocks and re-crystallized at room temperature from water (30%) / ethanol (70%) mixture. For MAS NMR experiments, the 5F-L-Trp sample was packed in a 1.3 mm MAS rotor.

### 2.2. MAS NMR spectroscopy

All experiments were performed at 11.7 T on Bruker Avance Neo and Avance III NMR spectrometers, equipped with wide-bore 0.7 mm HFX and 1.3 mm HFX MAS probes, respectively.  $^1H$  and  $^{19}F$  Larmor frequencies were 499.81 MHz and 470.29 MHz (Avance Neo spectrometer) and 500.13 MHz and 470.59 MHz (Avance III spectrometer), respectively. MAS frequency was controlled to  $\pm 10$  Hz by Bruker MAS III controller. The probe temperature was set to 235 K and corresponded to about 298 K at the sample.

For slow MAS experiments (10 kHz spinning frequency), a 1.3 mm HFX MAS probe was used. A direct polarization (DP)  $^{19}F$  spectrum was recorded for Mefloquine, using 8 scans, a recycle delay of 5 s, a pulse length of 2.35  $\mu s$ , and SPINAL-64 [33]  $^1H$  decoupling (85 kHz) during the acquisition period. For Atorvastatin calcium and 5F-L-Trp,  $^1H$ - $^{19}F$  cross polarization (CP) with a 82-100% linear ramp on  $^1H$  for  $^{19}F$  excitation was carried out. The  $^1H$  and  $^{19}F$  RF fields during the CP step were 75 and 45 kHz, respectively, and the contact time was 1.5 ms. The  $^{19}F$  Atorvastatin calcium spectrum was collected with 8,192 scans, a 8 s recycle delay, a  $^1H$  pulse length of 2.35  $\mu s$ , and SPINAL-64 [33]  $^1H$  decoupling (89 kHz) during the  $^{19}F$  acquisition period. For 5F-L-Trp, the  $^1H$  and  $^{19}F$  RF fields during the CP step were 77 and 48 kHz, respectively, and the contact time was 0.5 ms. The  $^{19}F$  5F-L-Trp spectrum was collected with 256 scans, a 4 s recycle delay, a  $^1H$  pulse length of 2.2  $\mu s$ , and SPINAL-64 [33]  $^1H$  decoupling (89 kHz) during  $^{19}F$  acquisition period.

Experiments with spinning frequencies  $\geq 60$  kHz were recorded using 0.7 mm HFX and 1.3 mm HFX probes, with  $^1H$  and  $^{19}F$   $\pi/2$  pulse lengths of 1.0 and 1.2  $\mu s$ , and 2.5 and 2.14  $\mu s$ , respectively. Low-power time-proportional-phase-modulation (TPPM)  $^1H$  decoupling during  $^{19}F$  acquisition [34] was employed, and the RF power was set to  $1/4$  the spinning frequency, 15, 20,

and 25 kHz at 60, 80, and 100 kHz MAS, respectively. For  $^1\text{H}$  decoupling during  $\text{RN}_n^v$  blocks, either a  $^1\text{H}$   $\pi$ -pulse was applied for every 'N' pulses ( $\pi$ -decoupling) or continuous-wave (CW) irradiation was employed with the RF power set to 1/2 of the MAS frequency. Here, heteronuclear decoupling is achieved by a homonuclear recoupling condition ('HORROR') shown to be effective due to the "self-decoupling" effect [35, 36].  $^{19}\text{F}$  chemical shifts are referenced with respect to trifluoroacetic acid (100  $\mu\text{M}$  in 25 mM sodium phosphate buffer, pH 6.5) as an external reference (0 ppm).

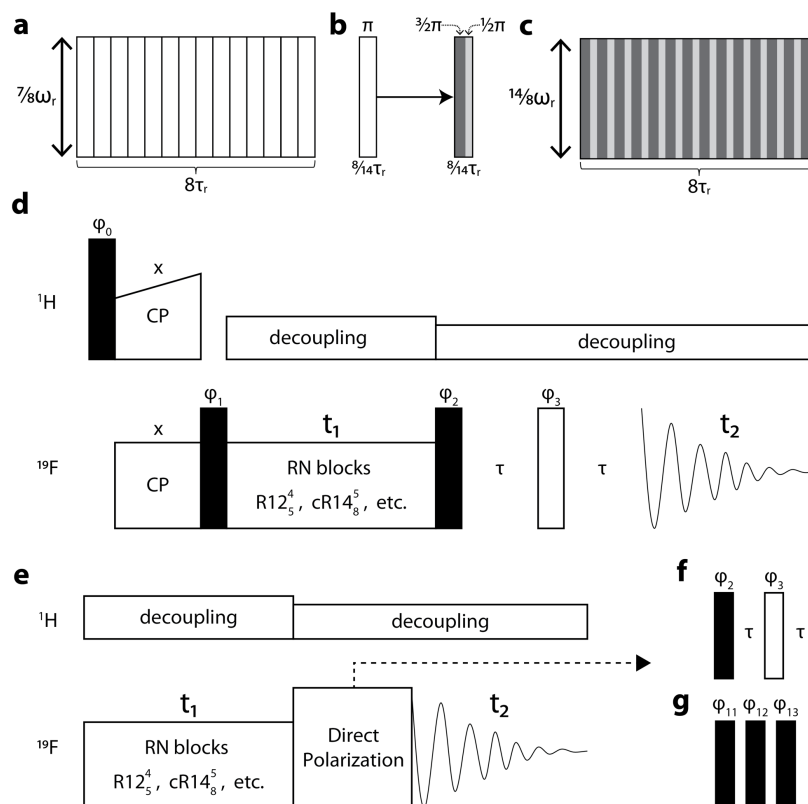


**Figure 1.** Schematic depiction of  $^{19}\text{F}$  RNCSA pulse sequences used. (a) One  $\text{R14}_8^5$  block. (b) Conversion of a single  $\pi$ -pulse to a  $270^\circ$ - $90^\circ$  composite pulse [37]. (c) One composite ( $270^\circ$ - $90^\circ$ )  $\text{R14}_8^5$  block. (d) CP-based  $^{19}\text{F}$  RNCSA with a short spin echo prior to acquisition for suppression of ring-down and baseline distortion. (e) DP-based  $^{19}\text{F}$  RNCSA experiment with either (f) spin echo or (g) triple pulse excitation [38] prior to acquisition for suppression of ring-down and baseline distortion. The spin echo-based  $^{19}\text{F}$  RNCSA phase cycle is:  $\varphi_0 = \text{yyyy -y-y-y-y}$ ;  $\varphi_1 = \text{yyyy -y-y-y-y}$ ;  $\varphi_2 = \text{x-xy-y}$ ;  $\varphi_3 = \text{xxxx yyyy -x-x-x-x -y-y-y-y}$ ;  $\varphi_{\text{rec}} = \text{x-y-xy -xyx-y}$ . The triple-pulse excitation phase cycle ( $\varphi_{11}$ ,  $\varphi_{12}$ ,  $\varphi_{13}$ ,  $\varphi_{\text{rec}}$ ) is as described in [38].

The  $^{19}\text{F}$  RNCSA pulse sequences used in this study are illustrated in Fig. 1. A single  $\text{R14}_8^5$   $t_1$  increment is shown in Fig 1a, a single R-symmetry  $\pi$  pulse and composite R-symmetry pulse [37] in Fig. 1b, and a single  $270^\circ$ - $90^\circ$  composite  $\text{R14}_8^5$  ( $\text{cR14}_8^5$ )  $t_1$  increment in Fig 1c. For Mefloquine and 5F-L-Trp spectra, 16 transients were summed over each  $t_1$  increment ( $d_w = n\tau_r$ ), and the recycle delays were 5 and 4 s, respectively. For the Atorvastatin calcium spectrum, a total of 64 transients were added for each  $t_1$  increment, and the recycle delay was 5 s. CP-based  $^{19}\text{F}$  RNCSA spectra were recorded for Atorvastatin calcium and 5F-L-Trp (Fig. 1d), and a DP-based spectrum for Mefloquine (Fig. 1e). CP-based  $^{19}\text{F}$  RNCSA experiments were performed with a 60-100% tangential ramp and a 80-100% linear ramp on  $^1\text{H}$  for Atorvastatin calcium and 5F-L-Trp,

respectively. For Atorvastatin, the  $^1\text{H}$  RF fields during CP were 156, 68, and 85 kHz at MAS frequencies of 60, 80, and 100 kHz, respectively, and the  $^{19}\text{F}$  RF fields were 96, 12, and 15 kHz at MAS frequencies of 60, 80, and 100 kHz, respectively. For 5F-L-Trp, the  $^1\text{H}$  and  $^{19}\text{F}$  RF fields during CP were 120 and 40 kHz, respectively, at a MAS frequency of 60 kHz. For ring-down suppression, a spin echo was implemented before the acquisition period in all DP-based experiments at 100 kHz MAS and all CP-based experiments at 60 and 100 kHz MAS (Fig. 1f). In DP-based experiments at 60 kHz MAS, triple-pulse excitation [38] (Fig. 1g) was used for the same purpose.

Considering the magnitude of  $^{19}\text{F}$  CSA and MAS frequencies used here, we selected R-symmetry pulse sequences that recouple the  $\sigma_2$ -spatial component of the CSA interaction. In these R-symmetry pulse sequences the scaling factor for homonuclear dipolar couplings is zero, and therefore  $^{19}\text{F}$ - $^{19}\text{F}$  dipolar couplings do not affect the recoupled line shape [27]. In addition, the  $\sigma_2$ -RNCSA sequences have a smaller scaling factor, thus they are better suited for the large  $^{19}\text{F}$  CSA values of 15-180 ppm as shown previously [13-15, 29]. The RF powers required for the R-symmetry pulse sequences used in this work are  $N/2n$  times the MAS frequency for  $\pi$ -pulse based sequences or  $N/n$  times the MAS frequency for composite sequences.

### 2.3. CSA convention

The CST parameters are defined according to the Haeberlen-Mehring-Spiess convention [39-41] as follows:

$$\delta_\sigma = \delta_{zz} - \delta_{iso} ; \eta = \frac{\delta_{yy} - \delta_{xx}}{\delta_{yy} - \delta_{iso}}$$

where  $\delta_{iso}$  is the isotropic shift,  $\delta_\sigma$  is the reduced anisotropy,  $\eta$  is the asymmetry parameter, and  $\delta_{ii}$  are the principal components of the CST.

### 2.4. Data processing

All 2D  $^{19}\text{F}$  RNCSA spectra were processed by Fourier transform in the direct dimension and real Fourier transform in the indirect dimension. No apodization was used.

### 2.5. $^{19}\text{F}$ RNCSA line shape fitting

All simulations were performed using the software package SIMPSON v4.2.1 and the 'opt' package for the fitting scripts [42, 43]. Simulations were performed for a single  $^{19}\text{F}$  spin system containing only the chemical shift interaction. Averaging was carried out over 678 REPULSION-distributed pairs of  $\{\alpha, \beta\}$  Euler angles with 8  $\gamma$  angles for the standard  $^{19}\text{F}$  RNCSA sequences, and 986 ZCW-distributed pairs of  $\{\alpha, \beta\}$  Euler angles with 8  $\gamma$  angles for the composite  $^{19}\text{F}$  RNCSA sequences. The fitting script optimized three parameters of the spin simulation:  $^{19}\text{F}$   $\delta_\sigma$ ,  $\eta$ , and exponential apodization. Other experimental parameters and those set by the R-symmetry numbers were fixed.

### 2.6. Spinning sideband analysis

For reference, the CSA parameters of Atorvastatin calcium [19], Mefloquine, and 5F-L-Trp were determined from slow MAS experiments through spinning sideband analysis. The CSA parameters were extracted by fitting the spinning sideband intensities using the Herzfeld-Berger analysis [44] as implemented in the HBA program [45].

### 3. Results and Discussion

$^{19}\text{F}$  CSA parameters were determined for Atorvastatin calcium by recording a CP-excitation spectrum at the MAS frequency of 10 kHz, and the  $\text{R}12_5^4$ -spectra at 60 and 100 kHz (Fig. 2). Atorvastatin calcium represents a relatively simple system with a weak  $^{19}\text{F}$  homonuclear dipolar coupling network, due to the low concentration (6% w/w) of the active pharmaceutical ingredient (API) in the formulation. The spectrum exhibits two narrow resonances with isotropic shifts of  $-40.1$  and  $-41.9$  ppm, consistent with our previous report [19]. The CSA parameters determined from the spinning sideband analysis of the slow-MAS spectrum and those extracted from the  $\text{R}12_5^4$ -spectra are in good agreement (Table 1). The fits for the  $^{19}\text{F}$ -RNCSA line shapes recorded at the MAS frequency of 60 kHz are somewhat better than those for the line shapes recorded at 100 kHz. The difference is due to the greater amount of sample packed in a 1.3 mm rotor compared to a 0.7 mm rotor, hence the higher sensitivity of the spectra recorded at the MAS frequency of 60 kHz.

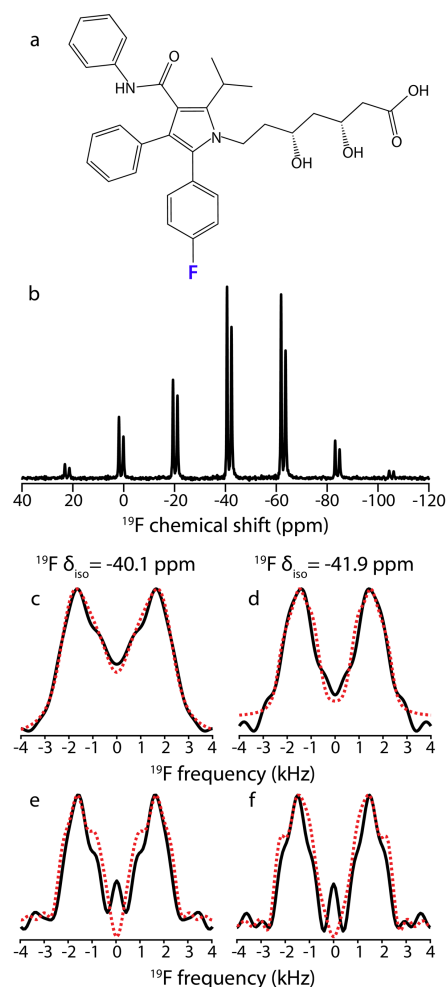


**Figure 2.** Spectrum and  $^{19}\text{F}$  CSA line shapes of Atorvastatin calcium (a) recorded with CP-excitation at the MAS frequency of 10 kHz (b) and  $\text{R}12_5^4$  RNCSA sequence at the MAS frequency of 60 kHz (c, d) and 100 kHz (e, f).  $^1\text{H}$   $\pi$ -decoupling was applied to remove  $^1\text{H}$ - $^{19}\text{F}$  dipolar couplings. The experimental spectra and the fits are shown in black solid lines and red dotted lines, respectively.  $\text{R}12_5^4$  spectra were recorded with 19 (60 kHz MAS) and 32 (100 kHz MAS)  $t_1$  transients, respectively, resulting in approximately the same CSA evolution period.

For microcrystalline 5F-L-Trp,  $^{19}\text{F}$  CSA parameters were extracted from a  $^1\text{H}$ - $^{19}\text{F}$  CP spectrum recorded at a MAS frequency of 10 kHz and from a  $\text{R}12_5^4$  spectrum acquired at a 60 kHz MAS frequency (Fig. 3, Table 2). Similar to Atorvastatin calcium, the  $^{19}\text{F}$  CSA parameters determined by both methods are within experimental error.

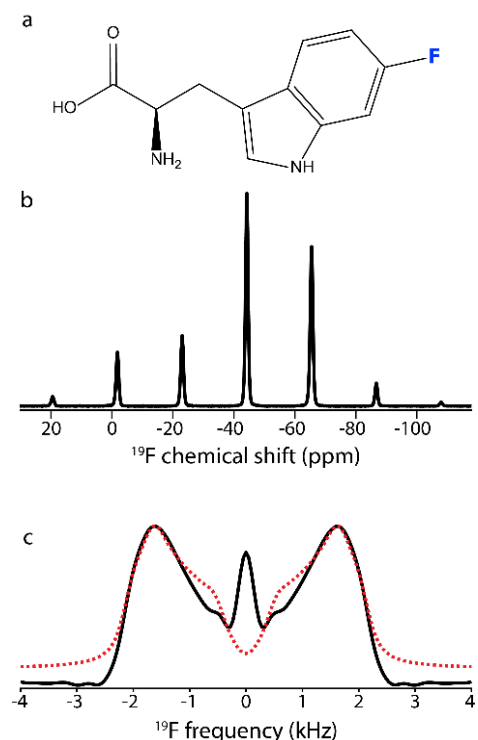


**Figure 3.** Spectrum and  $^{19}\text{F}$  CSA line shapes of 5F-L-Trp (a) recorded with  $^1\text{H}$ - $^{19}\text{F}$  CP at the MAS frequency of 10 kHz (b) and  $\text{R}12_5^4$  RNCSA acquired at 60 kHz MAS (c).  $^1\text{H}$   $\pi$ -decoupling was applied to remove  $^1\text{H}$ - $^{19}\text{F}$  dipolar couplings. The experimental spectra and the fits are shown in black solid and red dotted lines, respectively. The  $\text{R}12_5^4$  spectrum was collected with 38  $t_1$  transients.

In contrast to Atorvastatin and 5F-L-Trp, Mefloquine poses a challenge for CSA measurements using single-pulse excitation at slow MAS frequencies because of large homonuclear  $^{19}\text{F}$ - $^{19}\text{F}$  dipolar couplings of the  $\text{CF}_3$  groups, both intra- and intermolecular [46]. Indeed, the effect of these couplings is evident from the line widths observed at the MAS frequency of 10 kHz, see Fig. 4b. Therefore, we chose the  $\text{RN}_n^v$  sequences that recouple  $\sigma_2$ -CSA interactions while simultaneously decoupling homonuclear dipolar couplings. The CSA parameters extracted from  $\text{R}12_5^4$ -spectra recorded at MAS frequencies of 60 and 100 kHz are, therefore, more accurate than the slow-MAS parameters, see Fig. 4c,d and Table 3.

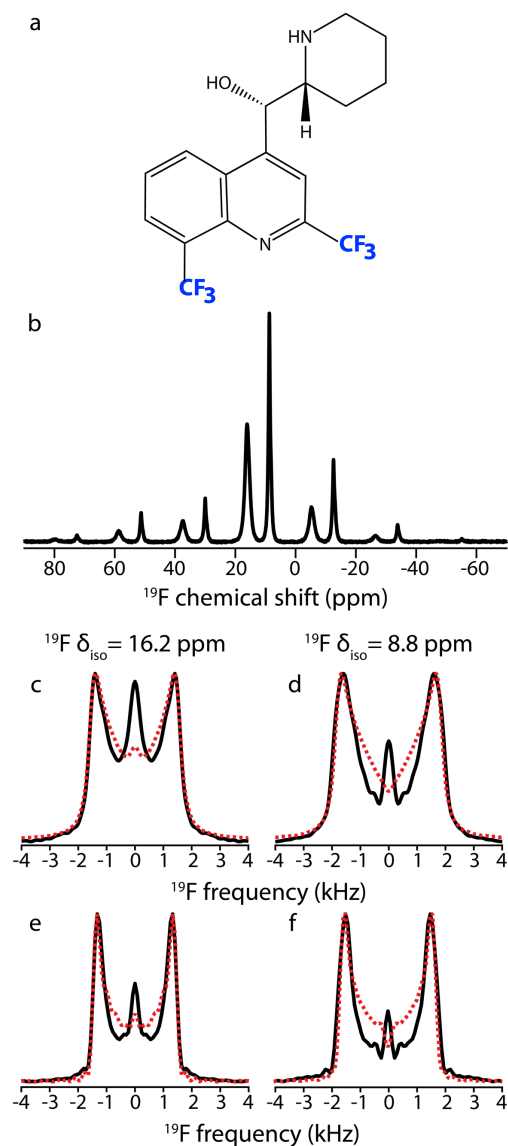


**Figure 4.**  $^{19}\text{F}$  spectrum and CSA line shapes of Mefloquine (a) recorded with single-pulse excitation at the MAS frequency of 10 kHz (b) and  $\text{R}12_5^4$  RNCSA acquired at 60 kHz (c, d) and 100 kHz (e, f).  $^1\text{H}$   $\pi$ -decoupling was applied to remove  $^1\text{H}$ - $^{19}\text{F}$  dipolar couplings. The experimental spectra and the fits are shown in black solid and red dotted lines, respectively.  $\text{R}12_5^4$  spectra were collected with 38 (MAS frequency of 60 kHz) and 64 (MAS frequency of 100 kHz)  $t_1$  transients, respectively, resulting in approximately the same CSA evolution period.

We also examined the effect of heteronuclear  $^1\text{H}$  decoupling on the Mefloquine  $^{19}\text{F}$  RNCSA line shapes acquired at the MAS frequency of 100 kHz. As shown in Fig. 5,  $^1\text{H}$  couplings result in considerable broadening of the RNCSA lines, which translates into larger experimental errors in both the reduced anisotropy (0.5-3 ppm, up to 6%) and asymmetry parameter (0.3-0.7 vs. 0.2-0.4) of the CST (Table 4). The choice of the decoupling scheme did not result in a noticeable difference: both,  $\pi$ -decoupling and CW irradiation were equally efficient. As a note, it should be mentioned that  $^1\text{H}$  decoupling will be most important at slower MAS frequencies for  $^{19}\text{F}$  RNCSA experiments in fully protonated systems.

Previously, Titman and coworkers postulated that  $^1\text{H}$ - $^{19}\text{F}$  dipolar couplings  $\geq 8.5$  kHz (corresponding to a distance shorter than  $\sim 2.35$  Å) adversely affect line shapes at a MAS frequency of 65 kHz [29]. However, their simulations did not consider the effect of an extensive dipolar coupled network of  $^1\text{H}$  spins. Such a network can introduce significant line broadening, as observed by us for Mefloquine, where, even at the MAS frequency of 100 kHz,  $^1\text{H}$  decoupling is necessary to eliminate these couplings. Conversely, it is possible that for systems devoid of protons (e.g., fully deuterated molecules) spinning at 100 kHz may not require  $^1\text{H}$  decoupling during  $^{19}\text{F}$  RNCSA experiments.

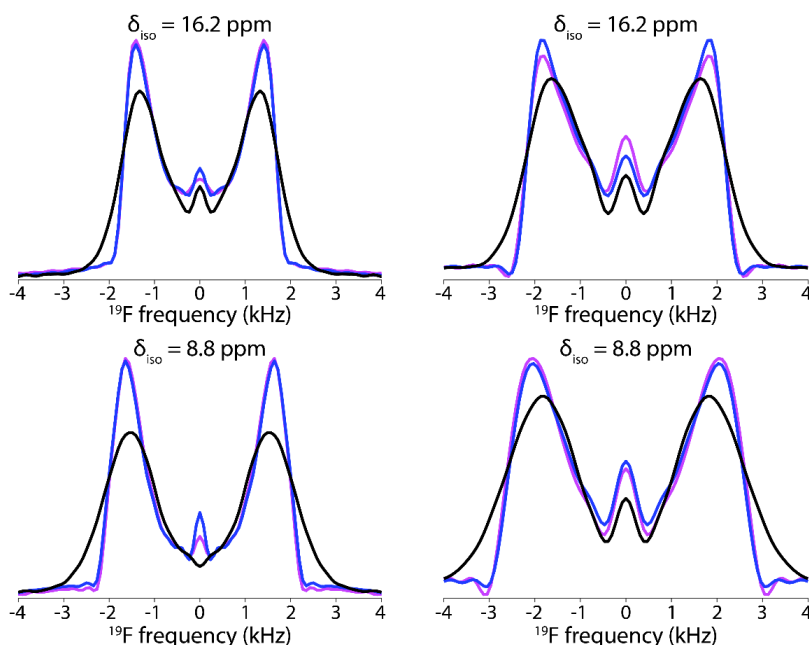


**Figure 5.** Effect of  $^1\text{H}$  decoupling on Mefloquine  $^{19}\text{F}$  RNCSA line shapes recorded at a MAS frequency of 100 kHz. Left and right are line shapes recorded with  $\text{R12}_5^4$  and  $\text{R14}_5^3$  sequences, respectively. Top and bottom are line shapes extracted for peaks with isotropic chemical shifts of 16.2 and 8.8 ppm, respectively. Line shapes recorded without and with  $\pi$ - and CW-decoupling are depicted in black, purple, and blue, respectively.  $\text{R12}_5^4$  and  $\text{R14}_5^3$  spectra were collected with 64 and 32  $t_1$  transients, respectively.

We therefore examined the performance of the  $^1\text{H}$ -decoupled  $^{19}\text{F}$  RNCSA at different MAS frequencies of 60, 80, and 100 kHz (Fig. 6). The recoupling efficiency increases with the increased spinning frequency, the relaxation-induced central peak decreases, and all features become narrower. Irrespective, the reduced anisotropy and asymmetry parameters extracted from the corresponding RNCSA line shapes all are within experimental error (Table 5).

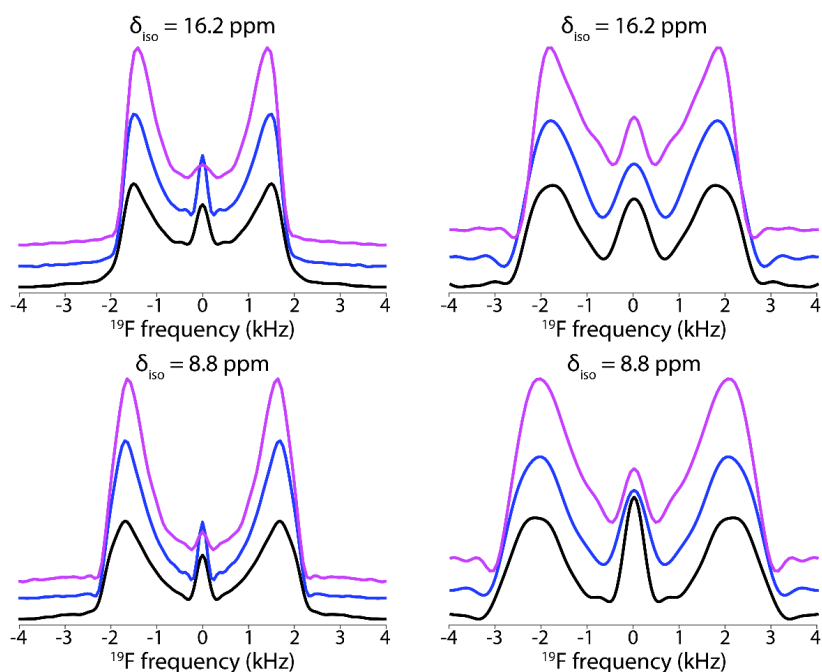


**Figure 6.**  $^1\text{H}$ -decoupled Mefloquine  $^{19}\text{F}$  RNCSA line shapes recorded at MAS frequencies of 100 kHz (purple), 80 kHz (blue), and 60 kHz (black). Left and right are  $\text{R}12_5^4$  and  $\text{R}14_5^3$  line shapes, respectively, and top and bottom are peaks with isotropic chemical shifts of 16.2 and 8.8 ppm, respectively.  $\pi$ -pulse  $^1\text{H}$  decoupling was applied in all experiments.  $\text{R}12_5^4$  spectra were collected with 38 (MAS frequency of 60 kHz), 51 (MAS frequency of 80 kHz), and 64 (MAS frequency of 100 kHz)  $t_1$  transients, respectively, resulting in approximately the same CSA evolution period.  $\text{R}14_5^3$  spectra were collected with 19 (MAS frequency of 60 kHz), 26 (MAS frequency of 80 kHz), and 32 (MAS frequency of 100 kHz)  $t_1$  transients, respectively, resulting in approximately the same CSA evolution period.

We also performed  $^{19}\text{F}$  RNCSA experiments using a broader range of R-symmetry numbers for recoupling the  $\sigma_2$ -spatial component of the CSA interaction while suppressing the homonuclear  $^{19}\text{F}$ - $^{19}\text{F}$  dipolar couplings. The following  $^{19}\text{F}$  RNCSA spectra at a MAS frequency of 60 kHz were recorded for Mefloquine and 5F-L-Trp:  $\text{R}10_9^3$ ,  $\text{R}10_7^1$ ,  $\text{R}12_7^4$ ,  $\text{R}14_8^5$ ,  $\text{R}20_9^8$ ,  $\text{R}14_6^5$ ,  $\text{R}12_5^4$ , and  $\text{R}14_5^3$ . In addition, we replaced the R-symmetry  $\pi$ -pulses in two sequences,  $\text{R}10_9^3$  and  $\text{R}14_8^5$ , with  $270^\circ$ - $90^\circ$  composite pulses [37] (Fig. 1b,c), in order to evaluate the performance of the  $\text{cR}10_9^3$  and  $\text{cR}14_8^5$  schemes on the line shapes (Fig. 7). Of the R-symmetry numbers tested, the  $\text{R}12_7^4$ ,  $\text{R}14_8^5$ ,  $\text{R}14_6^5$ ,  $\text{R}12_5^4$ ,  $\text{R}14_5^3$ , and  $\text{cR}14_8^5$  sequences worked well in all instances. Since low-power  $^{19}\text{F}$  RNCSA experiments possess small scaling factors [27],  $\text{R}12_7^4$  and  $\text{R}14_8^5$  sequences are expected to be better suited for larger  $^{19}\text{F}$  CSAs and/or higher magnetic fields.

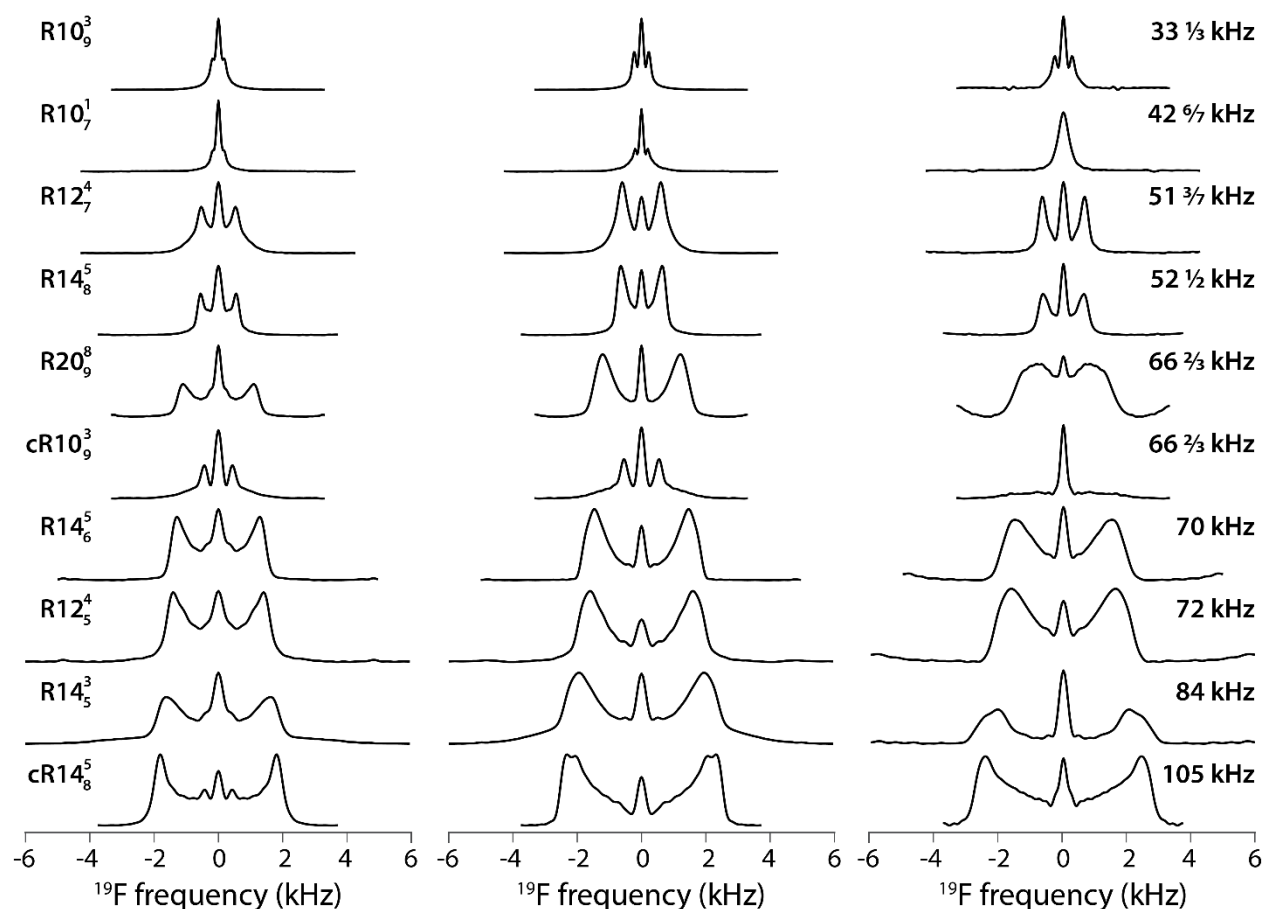


**Figure 7.**  $^{19}\text{F}$  RNCSA line shapes of Mefloquine and 5F-L-Trp at a MAS frequency of 60 kHz MAS using different R-symmetry sequences. The line shapes for two Mefloquine peaks at isotropic shifts 16.2 ppm (left) and 8.8 ppm (middle) as well as the line shapes for 5F-L-Trp (right) are shown. The R-symmetry numbers are indicated on the left and the corresponding RF power is indicated on the right. All spectra were collected with 38  $t_1$  transients, except for cR10 $_9^3$  and cR14 $_8^5$ , which were collected with 48 and 24  $t_1$  transients, respectively.  $^1\text{H}$   $\pi$ -decoupling was used during  $t_1$  evolution period of all sequences, but R14 $_5^3$  and cR14 $_8^5$ , for which by  $^1\text{H}$  CW-decoupling was employed.

The effect of a radio frequency (RF) field mismatch on the overall performance of  $^{19}\text{F}$  RNCSA experiments for the systems investigated here was evaluated. Prior studies reported that sensitivity to a RF mismatch depends on specific combinations of symmetry numbers in RN sequences [37, 47-50]. Here, we show that a RF field mismatch for the R12 $_7^4$ , R14 $_8^5$ , R14 $_6^5$ , R12 $_5^4$ , and R14 $_5^3$  experiments (Fig. 8 and Supplementary Table S1) affects all sequences to a very similar extent. The overall RF profile is non-linear and results in large errors in the measured CSA parameters when excessive RF power is applied. In practice, this indicates that for spectra that contain several  $^{19}\text{F}$  peaks dispersed over a large spectral width (a common case in  $^{19}\text{F}$  NMR since the chemical shift range is  $>300$  ppm), a single  $^{19}\text{F}$  RNCSA experiment will not suffice because of large off-resonance effects. In those instances, separate  $^{19}\text{F}$  RNCSA experiments need to be performed for different spectral regions with individual peaks set on resonance.

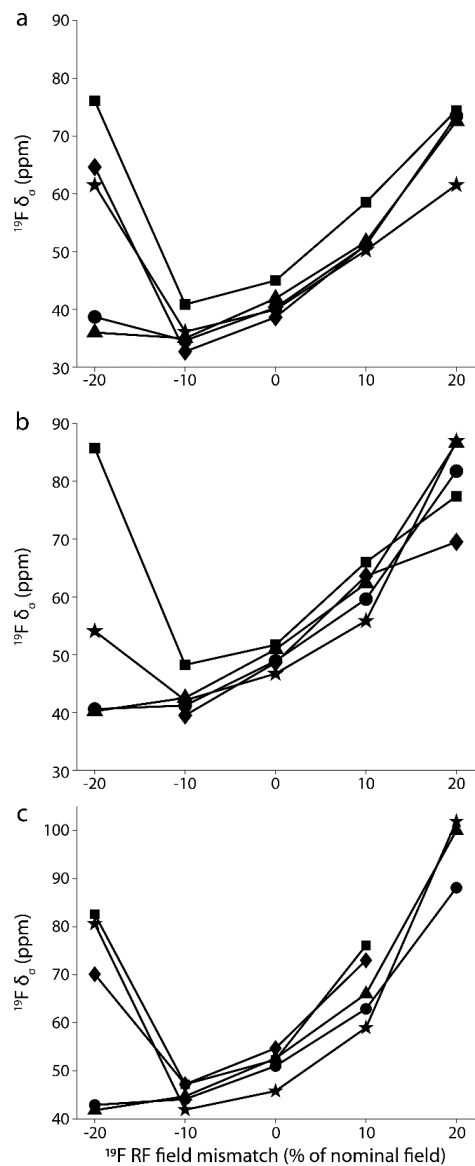


**Figure 8.** Effect of RF field mismatch on the  $^{19}\text{F}$  reduced anisotropy in RNCSA experiments of Mefloquine (peaks at 16.2 (a) and 8.8 (b) ppm) and microcrystalline 5F-L-Trp (c). All experiments were performed at a MAS frequency of 60 kHz.  $\delta_\sigma$  values extracted from R12 $_7^4$ , R14 $_8^5$ , R14 $_6^5$ , R12 $_5^4$ , and R14 $_5^3$  experiments are shown as squares, stars, circles, triangles, and diamonds, respectively. The number of  $t_1$  transients and  $^1\text{H}$  decoupling schemes are as described in the legend of Fig. 7. RF field mismatch effect was measured by recollecting the  $^{19}\text{F}$ -RNCSA experiment with an adjusted  $^{19}\text{F}$  RF field during the CSA recoupling period ( $t_1$ ), followed by fitting of the obtained line shapes.

The data shown in Fig. 8 reveal a large variation in  $\delta_\sigma$  values when RF power is mis-set to high values, while under-estimating the RF field has relatively modest effects on the spectra. When the RF power is within 10% of the correct value, the reduced anisotropy is still within experimental error (Supplementary Table S1). Similar effects were seen for the Atorvastatin calcium spectra recorded at a MAS frequency of 100 kHz (Fig. S1, Supplementary Table S2). The relatively small effect on the  $^{19}\text{F}$  RNCSA line shapes from under-estimating the RF field suggests that the  $B_1$  inhomogeneity plays a smaller role than RF field mismatch, since  $B_1$  inhomogeneity usually leads to lower effective RF fields away from the center of the coil [51].

To assess the off-resonance effects on  $^{19}\text{F}$  RNCSA line shapes, expected from the above RF field mismatch tests, we performed the  $\text{R12}_5^4$  experiment on Mefloquine with irradiation frequencies positioned on- and off-resonance (Fig. 9a-f). Irradiating 40 ppm off-resonance results in severely broadened recoupled line shapes, and at 80 ppm off complete loss of the RNCSA line shape is observed. Since a  $270^\circ$ - $90^\circ$  composite pulse had been reported to be more robust to an RF mismatch, albeit at the expense of significantly higher required RF power [37], we tested the  $\text{cR14}_8^5$  sequence on Mefloquine (Fig. 9g-l). Indeed, setting the irradiation frequency 40 ppm off resonance only modestly affects the recoupled line shape, while 80 ppm off-resonance irradiation results in an increased central peak. Fortunately, the reduced anisotropy and asymmetry parameters extracted from the spectra are within the experimental error (Table 6).

Of note is the intensity of the zero-frequency peak in the  $^{19}\text{F}$  RNCSA line shape, which progressively increases as the excitation pulses are set off resonance by 40 and 80 ppm. This peak originates from relaxation and/or experimental imperfections, such as RF field inhomogeneity and pulse imperfections. Interestingly, the relative contribution of the zero-frequency feature to the  $\text{cR14}_8^5$  line shape is relatively modest, attesting to the robustness of the composite pulse-based sequence.

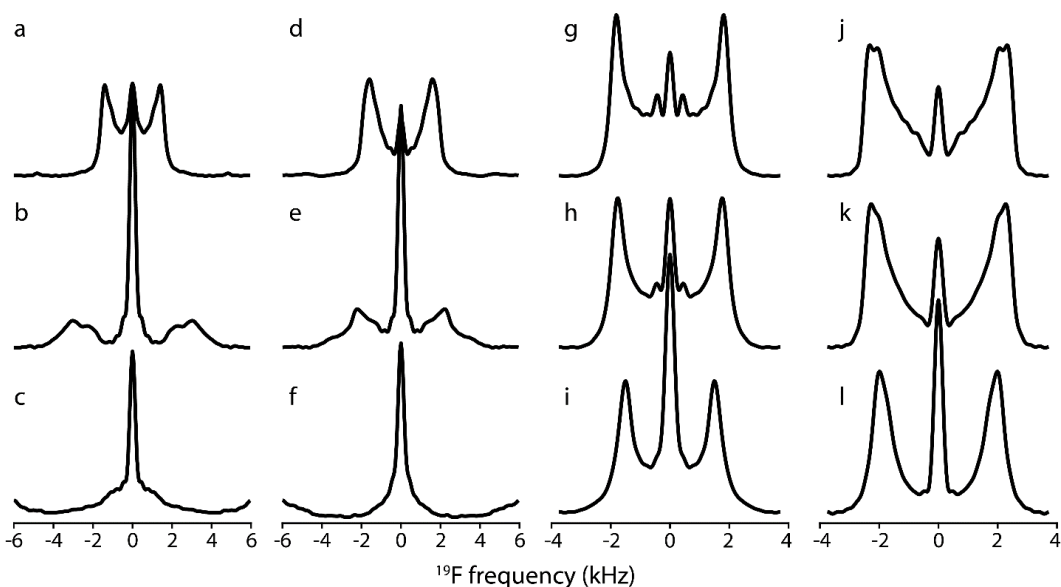


**Figure 9.** Off-resonance effects on the recoupled line shape in  $^{19}\text{F}$  RNCSA experiments of Mefloquine at a MAS frequency of 60 kHz.  $\text{R12}_5^4$  (a-f) and  $\text{cR14}_8^5$  (g-l) line shapes of Mefloquine peaks with isotropic shifts 16.2 ppm (a-c, g-i) and 8.8 ppm (d-f, j-l) with on-resonance irradiation at 13 ppm (a, d, g, j), 40 ppm off-resonance irradiation (b, e, h, k), and 80 ppm off-resonance irradiation (c, f, i, l).

We also evaluated the performance of the  $\text{cR14}_8^5$  experiment at a MAS frequency of 100 kHz for Mefloquine (Fig. 10 and Table 7). Comparison of the line shapes with those collected at 60 kHz reveals that the features are more distinct at the faster spinning frequency. In addition, the asymmetry of the CSA extracted at 100 kHz agrees better with the values observed using the  $\text{R12}_5^4$  experiment at 100 kHz MAS frequency (Table 3). Importantly, given the improved RF capabilities of the 0.7 HFXY MAS probe and the large spectral width of  $\text{cR14}_8^5$  at a MAS frequency

of 100 kHz, this sequence is advantageous for determining large  $^{19}\text{F}$  CSAs free of inaccuracies due to large RF mis-matches, as shown by simulated  $\text{cR14}_8^5$  line shapes (Fig. S2).

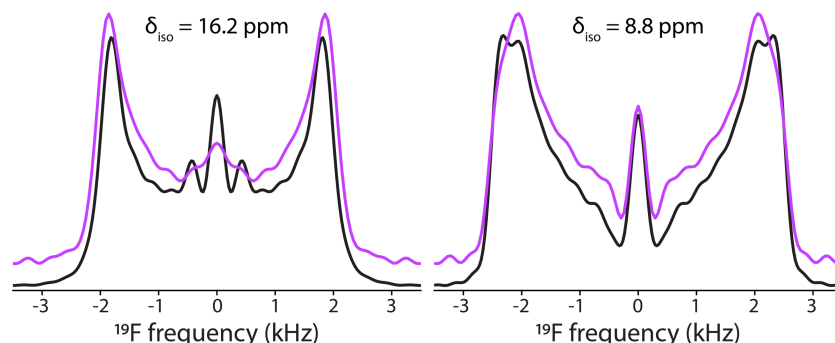


**Figure 10.**  $^1\text{H}$ -decoupled  $^{19}\text{F}$   $\text{cR14}_8^5$  line shapes of Mefloquine at MAS frequencies of 60 kHz (black) and 100 kHz (purple) for peaks with isotropic chemical shifts of 16.2 (left) and 8.8 ppm (right), respectively.  $\text{cR14}_8^5$  spectra were recorded with 24 (MAS frequency of 60 kHz and CW  $^1\text{H}$  decoupling) and 40 (MAS frequency of 100 kHz and  $\pi$ -pulse  $^1\text{H}$  decoupling)  $t_1$  transients, respectively, resulting in the same CSA evolution period.

#### 4. Conclusions

Accurate  $^{19}\text{F}$  CSA parameters were extracted from RNCSA experiments performed at high MAS frequencies of 60-100 kHz. These spinning frequencies are well suited for the recoupling of  $^{19}\text{F}$  CSA of most fluorinated aromatic and  $\text{CF}_3$  groups, common in pharmaceuticals and  $^{19}\text{F}$ -labeled proteins. For highly protonated systems,  $^1\text{H}$  decoupling is required, even at MAS frequencies as high as 100 kHz. While  $^{19}\text{F}$ -RNCSA is sensitive to RF mis-set and off-resonance effects, implementation of composite R-symmetry pulses makes the experiment more robust and, therefore, more accurate. The high-frequency  $^{19}\text{F}$ -RNCSA experiments presented and evaluated here open doors for accurate CSA measurements of homonuclear dipolar coupled  $^{19}\text{F}$  spins. We anticipate that the methodologies illustrated here for three select examples will find broad applications to a wide variety of fluorinated organic and biological molecules.

#### Acknowledgments

This work was supported by the National Science Foundation (NSF Grant CHE-1708773) and by the National Institutes of Health (NIH Grant P50AI150481, Technology Development Project 2). We acknowledge that support of the National Institutes of Health (NIH Grant P30GM110758) for the support of core instrumentation infrastructure at the University of Delaware. We thank Brent Runge and Kumar Tekwani Movellan for crystallizing the 5F-L-Trp sample.

#### Author contributions

T.P. and A.M.G. conceived the project and directed the work. T.P., J.S., C.M.Q., and G.P.-D. designed the MAS NMR experiments. G.P.-D., C.M.Q., and J.S. recorded the MAS NMR data. G.P.-D. analyzed the NMR data. All authors discussed the results. G.P.-D. and T.P. took the lead in writing the manuscript.

**Table 1.**  $^{19}\text{F}$  chemical shift anisotropy parameters of Atorvastatin calcium extracted from direct pulse excitation and RNCSA experiments.\*

| $\delta_{iso}$ (ppm) |                       | Direct excitation/<br>$\omega_r = 10$ kHz | R12 <sub>5</sub> <sup>4</sup> /<br>$\omega_r = 60$ kHz | R12 <sub>5</sub> <sup>4</sup> /<br>$\omega_r = 100$ kHz |
|----------------------|-----------------------|---|--|---|
| -40.1                | $\delta_\sigma$ (ppm) | 57.9                                      | 57.5   | 56.3  |
|                      | $\eta$                | 0.5                                       | 0.4  | 0.6   |
| -41.9                | $\delta_\sigma$ (ppm) | 55.2                                      | 53.9   | 53.4  |
|                      | $\eta$                | 0.6                                       | 0.7  | 0.8   |

\*The R12<sub>5</sub><sup>4</sup> spectra were recorded using 1.3 mm HFX (60 kHz) and 0.7 mm HFX (100 kHz) probes.

**Table 2.**  $^{19}\text{F}$  chemical shift anisotropy parameters of 5F-L-Trp extracted from direct pulse excitation and RNCSA experiments.\*

| $\delta_{iso}$ (ppm) |                       | Direct excitation/<br>$\omega_r = 10$ kHz | R12 <sub>5</sub> <sup>4</sup> /<br>$\omega_r = 60$ kHz |
|----------------------|-----------------------|---|--|
| -44.1                | $\delta_\sigma$ (ppm) | 53.3                                      | 52.3   |
|                      | $\eta$                | 0.1                                       | 0.4  |

\*The R12<sub>5</sub><sup>4</sup> spectra were recorded using a 1.3 mm HFX probe.

**Table 3.**  $^{19}\text{F}$  chemical shift anisotropy parameters of Mefloquine extracted from direct pulse excitation and RNCSA experiments.\*

| $\delta_{iso}$ (ppm) |                       | Direct excitation/<br>$\omega_r = 10$ kHz | R12 <sub>5</sub> <sup>4</sup> /<br>$\omega_r = 60$ kHz | R12 <sub>5</sub> <sup>4</sup> /<br>$\omega_r = 100$ kHz |
|----------------------|-----------------------|---|--|---|
| 16.2                 | $\delta_\sigma$ (ppm) | 37.5                                      | 41.8   | 39.3  |
|                      | $\eta$                | 0.3                                       | 0.1  | 0.1   |
| 8.8                  | $\delta_\sigma$ (ppm) | 40.4                                      | 49.5   | 44.7  |
|                      | $\eta$                | 0.2                                       | 0.0  | 0.3   |

\*The R12<sub>5</sub><sup>4</sup> spectra were recorded using 1.3 mm HFX (60 kHz) and 0.7 mm HFX (100 kHz) probes.

**Table 4.**  $^{19}\text{F}$  chemical shift anisotropy parameters of Mefloquine extracted from RNCSA experiments with and without  $^1\text{H}$  decoupling during the  $^{19}\text{F}$  RNCSA period, at 100 kHz MAS frequency.  $\pi$ , CW, and 'none' designate  $\pi$ -decoupling, CW-decoupling, and no  $^1\text{H}$  decoupling.

| $\delta_{iso}$ (ppm) |                       | $\text{R12}_5^4$ |      |      | $\text{R14}_5^3$ |      |      |
|----------------------|-----------------------|------------------|------|------|------------------|------|------|
|                      |                       | $\pi$            | CW   | none | $\pi$            | CW   | none |
| 16.2                 | $\delta_\sigma$ (ppm) | 43.1             | 43.2 | 44.3 | 44.7             | 44.5 | 44.0 |
|                      | $\eta$                | 0.2              | 0.2  | 0.3  | 0.4              | 0.4  | 0.4  |
| 8.8                  | $\delta_\sigma$ (ppm) | 51.3             | 52.0 | 54.5 | 51.6             | 52.7 | 52.0 |
|                      | $\eta$                | 0.4              | 0.4  | 0.7  | 0.4              | 0.3  | 0.6  |

**Table 5.**  $^{19}\text{F}$  chemical shift anisotropy parameters for Mefloquine extracted from RNCSA experiments at different MAS frequencies.

| $\delta_{iso}$ (ppm) |                         | R12 <sub>5</sub> <sup>4</sup> with $\pi$ -decoupling |        |        | R14 <sub>5</sub> <sup>3</sup> with $\pi$ -decoupling |        |        |
|----------------------|-------------------------|--|--------|--------|--|--------|--------|
|                      |                         | 100 kHz  | 80 kHz | 60 kHz | 100 kHz  | 80 kHz | 60 kHz |
| 16.2 ppm             | $\delta_{\sigma}$ (ppm) | 43.1   | 43.8   | 44.2   | 44.7   | 46.1   | 46.2   |
|                      | $\eta$                  | 0.2  | 0.1    | 0.1    | 0.4  | 0.4    | 0.4    |
| 8.8 ppm              | $\delta_{\sigma}$ (ppm) | 51.3   | 52.3   | 54.0   | 51.6   | 53.8   | 54.6   |
|                      | $\eta$                  | 0.4  | 0.2    | 0.4    | 0.4  | 0.5    | 0.6    |

**Table 6.**  $^{19}\text{F}$  chemical shift anisotropy parameters of Mefloquine extracted from cR14<sub>8</sub><sup>5</sup> experiments performed at a MAS frequency of 60 kHz for different on- and off-resonance irradiation frequencies .

| $\delta_{iso}$ (ppm) |                         | 40 ppm       |               | 80 ppm        |
|----------------------|-------------------------|--------------|---------------|---------------|
|                      |                         | On-resonance | off-resonance | off-resonance |
| 16.2 ppm             | $\delta_{\sigma}$ (ppm) | 36.5         | 36.0          | 32.2          |
|                      | $\eta$                  | 0.1          | 0.1           | 0.0           |
| 8.8 ppm              | $\delta_{\sigma}$ (ppm) | 45.9         | 45.4          | 41.1          |
|                      | $\eta$                  | 0.1          | 0.1           | 0.2           |

**Table 7.**  $^{19}\text{F}$  chemical shift anisotropy parameters of Mefloquine extracted from cR14<sub>8</sub><sup>5</sup> experiments performed at MAS frequencies of 60 and 100 kHz.\*

| $\delta_{iso}$ (ppm) |                         | 60 kHz | 100 kHz |
|----------------------|-------------------------|--------|---------|
| 16.2 ppm             | $\delta_{\sigma}$ (ppm) | 36.5   | 37.7    |
|                      | $\eta$                  | 0.1    | 0.2     |
| 8.8 ppm              | $\delta_{\sigma}$ (ppm) | 45.9   | 44.5    |
|                      | $\eta$                  | 0.1    | 0.3     |

\*The cR14<sub>8</sub><sup>5</sup> spectra were recorded using 1.3 mm HFX (60 kHz) and 0.7 mm HFX (100 kHz) probes.

## References

- [1] Y.G. Gakh, A.A. Gakh, A.M. Gronenborn, Fluorine as an NMR Probe for Structural Studies of Chemical and Biological Systems, *Magn. Reson. Chem.*, 38 (2000) 551-558.
- [2] H. Chen, S. Viel, F. Ziarelli, L. Peng,  $^{19}\text{F}$  NMR: A Valuable Tool for Studying Biological Events, *Chem. Soc. Rev.*, 42 (2013) 7971-7982.
- [3] A.M. Gronenborn, Small, but Powerful and Attractive:  $^{19}\text{F}$  in Biomolecular NMR, *Structure*, 30 (2021) 6-14.
- [4] Y. Zhou, J. Wang, Z. Gu, S. Wang, W. Zhu, J.L. Aceña, V.A. Soloshonok, K. Izawa, H. Liu, Next Generation of Fluorine-Containing Pharmaceuticals, Compounds Currently in Phase II–III Clinical Trials of Major Pharmaceutical Companies: New Structural Trends and Therapeutic Areas, *Chem. Rev.*, 116 (2016) 422-518.
- [5] H. Mei, J. Han, S. Fustero, M. Medio-Simon, D.M. Sedgwick, C. Santi, R. Ruzziconi, V.A. Soloshonok, Fluorine-Containing Drugs Approved by the FDA in 2018, *Chem. Eur. J.*, 25 (2019) 11797-11819.
- [6] M. Inoue, Y. Sumii, N. Shibata, Contribution of Organofluorine Compounds to Pharmaceuticals, *ACS Omega*, 5 (2020) 10633-10640.
- [7] L. Liang, Y. Ji, K. Chen, P. Gao, Z. Zhao, G. Hou, Solid-State NMR Dipolar and Chemical Shift Anisotropy Recoupling Techniques for Structural and Dynamical Studies in Biological Systems, *Chem. Rev.*, 10.1021/acs.chemrev.1c00779 (2022).
- [8] M. Mehring, R.G. Griffin, J.S. Waugh,  $^{19}\text{F}$  Shielding Tensors from Coherently Narrowed NMR Powder Spectra, *J. Chem. Phys.*, 55 (1971) 746-755.
- [9] A.N. Garroway, D.C. Stalker, P. Mansfield,  $^{19}\text{F}$  Chemical Shift Anisotropy in Aligned PTFE Fibres, *Polymer*, 16 (1975) 161-165.
- [10] S.L. Grage, J. Wang, T.A. Cross, A.S. Ulrich, Solid-State  $^{19}\text{F}$ -NMR Analysis of  $^{19}\text{F}$ -Labeled Tryptophan in Gramicidin A in Oriented Membranes, *Biophys. J.*, 83 (2002) 3336-3350.
- [11] Y. Su, W.F. DeGrado, M. Hong, Orientation, Dynamics, and Lipid Interaction of an Antimicrobial Arylamide Investigated by  $^{19}\text{F}$  and  $^{31}\text{P}$  Solid-State NMR Spectroscopy, *J. Am. Chem. Soc.*, 132 (2010) 9197-9205.
- [12] J. Salgado, S.L. Grage, L.H. Kondejewski, R.S. Hodges, R.N. McElhaney, A.S. Ulrich, Membrane-Bound Structure and Alignment of the Antimicrobial  $\beta$ -Sheet Peptide Gramicidin S Derived from Angular and Distance Constraints by Solid State  $^{19}\text{F}$ -NMR, *J. Biomol. NMR*, 21 (2001) 191-208.
- [13] T.-W. Su, D.-L.M. Tzou, Solid-State Fast Magic Angle Spinning  $^{19}\text{F}$  NMR Studies of Morphology in Poly(Vinylidene Fluoride), *Polymer*, 41 (2000) 7289-7293.
- [14] U.H.N. Dürr, S.L. Grage, R. Witter, A.S. Ulrich, Solid State  $^{19}\text{F}$  NMR Parameters of Fluorine-Labeled Amino Acids. Part I: Aromatic Substituents, *J. Magn. Reson.*, 191 (2008) 7-15.
- [15] S.L. Grage, U.H.N. Dürr, S. Afonin, P.K. Mikhailiuk, I.V. Komarov, A.S. Ulrich, Solid State  $^{19}\text{F}$  NMR Parameters of Fluorine-Labeled Amino Acids. Part II: Aliphatic Substituents, *J. Magn. Reson.*, 191 (2008) 16-23.
- [16] M. Roos, T. Wang, A.A. Shcherbakov, M. Hong, Fast Magic-Angle-Spinning  $^{19}\text{F}$  Spin Exchange NMR for Determining Nanometer  $^{19}\text{F}$ – $^{19}\text{F}$  Distances in Proteins and Pharmaceutical Compounds, *J. Phys. Chem. B*, 122 (2018) 2900-2911.
- [17] M. Wang, M. Lu, M.P. Fritz, C.M. Quinn, I.-J.L. Byeon, C.-H. Byeon, J. Struppe, W. Maas, A.M. Gronenborn, T. Polenova, Fast Magic-Angle Spinning  $^{19}\text{F}$  NMR Spectroscopy of HIV-1 Capsid Protein Assemblies, *Angew. Chem. Int. Ed.*, 57 (2018) 16375-16379.
- [18] B. Kwon, M. Roos, V.S. Mandala, A.A. Shcherbakov, M. Hong, Elucidating Relayed Proton Transfer through a His–Trp–His Triad of a Transmembrane Proton Channel by Solid-State NMR, *J. Mol. Biol.*, 431 (2019) 2554-2566.
- [19] C.M. Quinn, R. Zadorozhnyi, J. Struppe, I.V. Sergeyev, A.M. Gronenborn, T. Polenova, Fast  $^{19}\text{F}$  Magic-Angle Spinning Nuclear Magnetic Resonance for the Structural Characterization of Active Pharmaceutical Ingredients in Blockbuster Drugs, *Anal. Chem.*, 93 (2021) 13029-13037.

- [20] A.A. Shcherbakov, M. Hong, Rapid Measurement of Long-Range Distances in Proteins by Multidimensional  $^{13}\text{C}$ - $^{19}\text{F}$  REDOR NMR under Fast Magic-Angle Spinning, *J. Biomol. NMR*, 71 (2018) 31-43.
- [21] M. Lu, S. Sarkar, M. Wang, J. Kraus, M. Fritz, C.M. Quinn, S. Bai, S.T. Holmes, C. Dybowski, G.P.A. Yap, J. Struppe, I.V. Sergeyev, W. Maas, A.M. Gronenborn, T. Polenova,  $^{19}\text{F}$  Magic Angle Spinning NMR Spectroscopy and Density Functional Theory Calculations of Fluorosubstituted Tryptophans: Integrating Experiment and Theory for Accurate Determination of Chemical Shift Tensors, *J. Phys. Chem. B*, 122 (2018) 6148-6155.
- [22] U. Scheler, R.K. Harris, Fluorine-19 NMR of Solids with Both Homonuclear (Multipulse) Decoupling and Pulsed Proton Decoupling, *Chem. Phys. Lett.*, 262 (1996) 137-141.
- [23] Q. Chen, K. Schmidt-Rohr, Backbone Dynamics of the Nafion Ionomer Studied by  $^{19}\text{F}$ - $^{13}\text{C}$  Solid-State NMR, *Macromol. Chem. Phys.*, 208 (2007) 2189-2203.
- [24] M.H. Levitt, Symmetry-Based Pulse Sequences in Magic-Angle Spinning Solid-State NMR, in: D.M. Grant, R.K. Harris (Eds.) *Encyclopedia of Magnetic Resonance*, John Wiley & Sons Ltd, Chichester, UK, 2002, pp. 165-196.
- [25] X. Zhao, M. Edén, M.H. Levitt, Recoupling of Heteronuclear Dipolar Interactions in Solid-State NMR Using Symmetry-Based Pulse Sequences, *Chem. Phys. Lett.*, 342 (2001) 353-361.
- [26] M. Carravetta, M. Edén, X. Zhao, A. Brinkmann, M.H. Levitt, Symmetry Principles for the Design of Radiofrequency Pulse Sequences in the Nuclear Magnetic Resonance of Rotating Solids, *Chem. Phys. Lett.*, 321 (2000) 205-215.
- [27] G. Hou, I.-J.L. Byeon, J. Ahn, A.M. Gronenborn, T. Polenova, Recoupling of Chemical Shift Anisotropy by R-Symmetry Sequences in Magic Angle Spinning NMR Spectroscopy, *J. Chem. Phys.*, 137 (2012) 134201.
- [28] G. Hou, S. Paramasivam, I.-J.L. Byeon, A.M. Gronenborn, T. Polenova, Determination of Relative Tensor Orientations by  $\gamma$ -Encoded Chemical Shift Anisotropy/Heteronuclear Dipolar Coupling 3D NMR Spectroscopy in Biological Solids, *Phys. Chem. Chem. Phys.*, 12 (2010) 14873-14883.
- [29] F. Martini, H.K. Miah, D. Iuga, M. Geppi, J.J. Titman, Measuring  $^{19}\text{F}$  Shift Anisotropies and  $^1\text{H}$ - $^{19}\text{F}$  Dipolar Interactions with Ultrafast MAS NMR, *J. Magn. Reson.*, 259 (2015) 102-107.
- [30] G. Anderluh, A. Razpotnik, Z. Podlesek, P. Maček, F. Separovic, R.S. Norton, Interaction of the Eukaryotic Pore-Forming Cytolysin Equinatoxin II with Model Membranes:  $^{19}\text{F}$  NMR Studies, *J. Mol. Biol.*, 347 (2005) 27-39.
- [31] B. Kwon, T. Mandal, M.R. Elkins, Y. Oh, Q. Cui, M. Hong, Cholesterol Interaction with the Trimeric HIV Fusion Protein gp41 in Lipid Bilayers Investigated by Solid-State NMR Spectroscopy and Molecular Dynamics Simulations, *J. Mol. Biol.*, 432 (2020) 4705-4721.
- [32] M. Lu, R. Ishima, T. Polenova, A.M. Gronenborn,  $^{19}\text{F}$  NMR Relaxation Studies of Fluorosubstituted Tryptophans, *J. Biomol. NMR*, 73 (2019) 401-409.
- [33] B.M. Fung, A.K. Khitrin, K. Ermolaev, An Improved Broadband Decoupling Sequence for Liquid Crystals and Solids, *J. Magn. Reson.*, 142 (2000) 97-101.
- [34] M. Kotecha, N.P. Wickramasinghe, Y. Ishii, Efficient Low-Power Heteronuclear Decoupling in  $^{13}\text{C}$  High-Resolution Solid-State NMR under Fast Magic Angle Spinning, *Magn. Reson. Chem.*, 45 (2007) S221-S230.
- [35] G.D. Paëpe, B. Eléna, L. Emsley, Characterization of Heteronuclear Decoupling through Proton Spin Dynamics in Solid-State Nuclear Magnetic Resonance Spectroscopy, *J. Chem. Phys.*, 121 (2004) 3165-3180.
- [36] M. Ernst, A. Samoson, B.H. Meier, Decoupling and Recoupling Using Continuous-Wave Irradiation in Magic-Angle-Spinning Solid-State NMR: A Unified Description Using Bimodal Floquet Theory, *J. Chem. Phys.*, 123 (2005) 064102.
- [37] M.K. Pandey, M. Malon, A. Ramamoorthy, Y. Nishiyama, Composite- $180^\circ$  Pulse-Based Symmetry Sequences to Recouple Proton Chemical Shift Anisotropy Tensors under Ultrafast MAS Solid-State NMR Spectroscopy, *J. Magn. Reson.*, 250 (2015) 45-54.

- [38] F. Wang, S.K. Ramakrishna, P. Sun, R. Fu, Triple-Pulse Excitation: An Efficient Way for Suppressing Background Signals and Eliminating Radio-Frequency Acoustic Ringing in Direct Polarization NMR Experiments, *J. Magn. Reson.*, 332 (2021) 107067.
- [39] U. Haeberlen, *Advances in Magnetic Resonance*, Academic Press, New York, 1976.
- [40] M. Mehring, *Principles of High Resolution NMR in Solids*, Springer Verlag, Berlin, 1983.
- [41] H. Spiess, *NMR Basic Principles and Progress*, Springer Verlag, Berlin, 1978.
- [42] M. Bak, J.T. Rasmussen, N.C. Nielsen, SIMPSON: A General Simulation Program for Solid-State NMR Spectroscopy, *J. Magn. Reson.*, 147 (2000) 296-330.
- [43] Z. Tošner, R. Andersen, B. Stevansson, M. Edén, N.C. Nielsen, T. Vosegaard, Computer-Intensive Simulation of Solid-State NMR Experiments Using SIMPSON, *J. Magn. Reson.*, 246 (2014) 79-93.
- [44] J. Herzfeld, A.E. Berger, Sideband Intensities in NMR Spectra of Samples Spinning at the Magic Angle, *J. Chem. Phys.*, 73 (1980) 6021-6030.
- [45] Hba 1.8.1, K. Eichele, Universität Tübingen, 2021
- [46] C. Guo, M.P. Fritz, J. Struppe, S. Wegner, J. Stringer, I.V. Sergeyev, C.M. Quinn, A.M. Gronenborn, T. Polenova, Fast  $^{19}\text{F}$  Magic Angle Spinning NMR Crystallography for Structural Characterization of Fluorine-Containing Pharmaceutical Compounds, *Anal. Chem.*, 93 (2021) 8210-8218.
- [47] G. Hou, X. Lu, A.J. Vega, T. Polenova, Accurate Measurement of Heteronuclear Dipolar Couplings by Phase-Alternating R-Symmetry (PARS) Sequences in Magic Angle Spinning NMR Spectroscopy, *J. Chem. Phys.*, 141 (2014) 104202.
- [48] G. Hou, I.-J.L. Byeon, J. Ahn, A.M. Gronenborn, T. Polenova,  $^1\text{H}$ - $^{13}\text{C}$ / $^1\text{H}$ - $^{15}\text{N}$  Heteronuclear Dipolar Recoupling by R-Symmetry Sequences under Fast Magic Angle Spinning for Dynamics Analysis of Biological and Organic Solids, *J. Am. Chem. Soc.*, 133 (2011) 18646-18655.
- [49] X. Lu, H. Zhang, M. Lu, A.J. Vega, G. Hou, T. Polenova, Improving Dipolar Recoupling for Site-Specific Structural and Dynamics Studies in Biosolids NMR: Windowed RN-Symmetry Sequences, *Phys. Chem. Chem. Phys.*, 18 (2016) 4035-4044.
- [50] F. Rossi, N.T. Duong, M.K. Pandey, M.R. Chierotti, R. Gobetto, Y. Nishiyama, Determination of the  $^{15}\text{N}$  Chemical Shift Anisotropy in Natural Abundance Samples by Proton-Detected 3D Solid-State NMR under Ultrafast MAS of 70 kHz, *Magn. Reson. Chem.*, 57 (2019) 294-303.
- [51] Z. Tošner, A. Porea, J.O. Struppe, S. Wegner, F. Engelke, S.J. Glaser, B. Reif, Radiofrequency Fields in MAS Solid State NMR Probes, *J. Magn. Reson.*, 284 (2017) 20-32.